Water Oxidation by Mononuclear Ruthenium Complexes with TPA-Based Ligands

Bhasker Radaram,[†] Jeffrey A. Ivie,[‡] Wangkheimayum Marjit Singh,[†] Rafal M. Grudzien,[†] Joseph H. Reibenspies,[§] Charles Edwin Webster,*,[†] and Xuan Zhao*,[†]

[†]Department of Chemistry, The University of Memphis, Memphis, Tennessee 38152, United States

[‡]Department of Chemistry, Physics, and Astronomy, Georgia College & State University, Milledgeville, Georgia 31061, United States

[§]Department of Chemistry, Texas A&M University, College Station, Texas 77843-3255, United States

Ⓢ Supporting Information

ABSTRACT: The synthesis, characterization, and water oxidation activity of mononuclear ruthenium complexes with tris(2-pyridylmethyl)amine (TPA), tris(6-methyl-2-pyridylmethyl)amine (Me$_3$TPA), and a new pentadentate ligand *N,N*-bis(2-pyridinylmethyl)-2,2′-bipyridine-6-methanamine (DPA-Bpy) have been described. The electrochemical properties of these mononuclear Ru complexes have been investigated by both experimental and computational methods. Using Ce^{IV} as oxidant, stoichiometric oxidation of water by [Ru(TPA)(H$_2$O)$_2$]$^{2+}$ was observed, while Ru(Me$_3$TPA)(H$_2$O)$_2$]$^{2+}$ has much less activity for water oxidation. Compared to [Ru(TPA)(H$_2$O)$_2$]$^{2+}$ and [Ru(Me$_3$TPA)(H$_2$O)$_2$]$^{2+}$, [Ru(DPA-Bpy)(H$_2$O)]$^{2+}$ exhibited 20 times higher activity for water oxidation. This study demonstrates a new type of ligand scaffold to support water oxidation by mononuclear Ru complexes.

$$2H_2O + 4Ce^{IV} \longrightarrow O_2 + 4H^+ + 4Ce^{III}$$
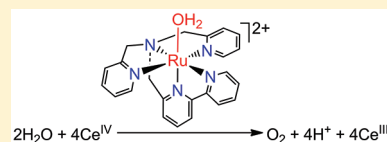
INTRODUCTION

Oxidation of water to molecular oxygen is a reaction of vital importance to sustain life on earth.[1] Using the energy from sunlight, photosynthesis splits water into oxygen and extracts electrons from water to reduce carbon dioxide into carbohydrates.[2] Design of water oxidation catalysts represents a critical step in artificial photosynthesis for conversion and storage of sunlight into high-energy chemicals such as H$_2$.[3] Synthetic structural and functional models of the oxygen-evolving center (OEC) in Photosystem II (PSII) have offered important insight into the water oxidation process catalyzed by the OEC.[4] It has been generally recognized that high-valent metal—oxo species, such as Mn═O, Ru═O, and Co═O, are involved in splitting of the water molecule to produce molecular dioxygen.[5] Ru complexes have played an important role in developing water oxidation catalysts. The dinuclear *cis,cis*-[(bpy)$_2$(H$_2$O)RuORu(H$_2$O)(bpy)$_2$]$^{4+}$ complex known as "blue dimer" was the first molecular complex discovered to catalytically oxidize water to dioxygen.[5e] Over the past few years, a number of other types of dinuclear and mononuclear Ru complexes capable of oxidizing water to molecular dioxygen have been designed, synthesized, and characterized.[6]

Tetradentate ligand tris(2-pyridylmethyl)amine (TPA) and its derivatives have been used extensively in modeling the active sites of mono- and dinuclear nonheme metalloproteins involved in dioxygen activation, such as Fe-, Cu-, and Ni-containing metalloproteins.[7] Ru complexes with TPA ligand have also received much attention.[8] Formation of high-valent Ru═O species has been reported for ruthenium complexes with TPA ligand.[9] For example, mononuclear [Ru(TPA)(H$_2$O)$_2$]$^{2+}$ (**1a**) can achieve redox states from Ru^{II} to Ru^{VI} through a proton-coupled electron transfer process. Oxygenation of hydrocarbons by

Ru═O species has been reported.[9] Since TPA is a tetradentate ligand, it provides a scaffold to design novel types of penta- and hexadentate ligands and offers the opportunity to include a second-coordination sphere environment to tune the activity of metal complexes. We are interested in exploring the activity of water oxidation by high-valent Ru═O complexes based on TPA ligand. Here, we describe the synthesis, characterization, and water oxidation activity of mononuclear Ru complexes with TPA and its derivatives (Figure 1).

EXPERIMENTAL SECTION

Materials and Synthesis. All chemicals were purchased from Sigma-Aldrich except noted. The reagent *N*-bromosuccinimide (NBS) was purified by recrystallization from boiling water before use. Other reagents such as 2-(aminomethyl)pyridine, 2,6-lutidine, benzoyl peroxide, potassium phthalimide, RuCl$_3$·3H$_2$O, (NH$_4$)$_2$Ce(NO$_3$)$_6$, and 6-methyl-2,2′-dipyridyl were used as received without further purification. Milli-Q H$_2$O (18.2 MΩ) was used in all experiments. H$_2$O^{18} was obtained from Cambridge Isotope Inc. Syntheses of tris(2-pyridylmethyl)amine (TPA), tris(6-methyl-2-pyridylmethyl)amine (Me$_3$TPA), and 6-(bromomethyl)-2,2′-bipyridine were carried out following literature methods.[10] [Ru(TPA)(H$_2$O)$_2$](PF$_6$)$_2$ (**1a**) was synthesized according to the literature method.[9]

Synthesis of *N,N*-Bis(2-pyridinylmethyl)-2,2′-bipyridine-6-methanamine (DPA-Bpy). To a solution of 6-(bromomethyl)-2,2′-bipyridine (0.66 g, 2.65 mmol) in acetonitrile (50 mL) was added 1 equiv of di-(2-picolyl)amine (0.52 g, 2.65 mmol) at room temperature. The base di-isopropyl ethyl amine (0.69 mL, 3.98 mmol) was added
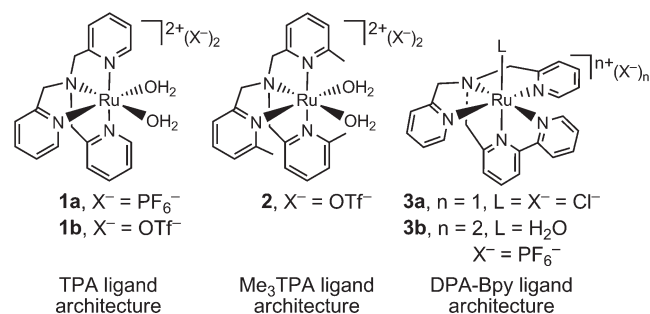
Figure 1. Mononuclear Ru complexes.

dropwise at 0 °C. The reaction mixture was stirred at room temperature for 5 h, and the reaction progress was monitored by TLC. Upon completion of the reaction, water (50 mL) was added. The product was extracted into ethyl acetate (3 × 50 mL) and washed with brine (2 × 30 mL). The combined organic layers were dried over anhydrous Na_2SO_4, filtered, and evaporated under reduced pressure to afford the crude compound. Recrystallization in hexane yielded a white solid (0.8 g, 81%). ^{1}H NMR (CDCl$_3$, 500 MHz): δ 3.88 (s, 4H, pyridyl methylene, H1), δ 3.90 (s, 2H, bipyridyl methylene, H6), 7.07 (dt, J = 5.76 Hz, 2H, py-H4), 7.21 (dt, J = 8.4 Hz, 1H, bpy-H12), 7.46 (d, J = 8.0 Hz, 1H, bpy-H7), 7.59 (d, J = 6.5 Hz, 2H, py-H2), 7.60 (d, J = 6.5 Hz, 2H, py-H3), 7.71 (dt, J = 7.5 Hz, 1H, bpy-H8), 7.73 (dt, J = 7.5 Hz, 1H, bpy-H11), 8.17 (d, J = 7.5 Hz, 1H, bpy-H9), 8.36 (d, J = 8.0 Hz, 1H, bpy-H10), 8.46 (d, J = 5 Hz, 2H, py-H5), 8.58 (d, J = 5.0 Hz, 1H, bpy-H13). Anal. Calcd for $C_{23}H_{21}N_5$: C, 75.18; H, 5.76; N, 19.06. Found: C, 75.01; H, 5.85; N, 18.89.

[Ru(TPA)(H$_2$O)$_2$](CF$_3$SO$_3$)$_2$·H$_2$O (1b). To a refluxed solution of RuCl$_3$·3H$_2$O (0.20 g, 0.764 mmol) in ethanol (30 mL) was added TPA (0.222 g, 0.764 mmol). After refluxing for 10 min, 20 mL of an aqueous solution of AgCF$_3$SO$_3$ (0.588 g, 2.294 mmol) was added. The mixture was then refluxed for 24 h, and the precipitate was removed by filtration. After removal of solvent, the product was dissolved in a minimum amount of ethanol and filtered. After washing with ether and drying under vacuum, a dark green solid was obtained. Yield: 0.19 g (33%). ^{1}H NMR (270 MHz, CD$_3$CN): δ 4.56 (s, 2H, CH$_2$ (axial)), 4.87–5.09 (ABq, J_{AB} = 15.47 Hz, 4H, CH$_2$ (equatorial), 7.04 (d, J = 7.91 Hz, 1H, Pyr-H3 (axial)), 7.23 (t, J = 6.54 Hz, Pyr-H5 (axial)), 7.31 (t, 6.6 Hz, 2H, Pyr-H5 (equatorial)), 7.47 (d, J = 7.91 Hz, 2H, Pyr-H3 (equatorial)), 7.59 (t, J = 15.57 Hz, 1H, Pyr-H4 (axial)), 7.80 (t, J = 15.57 Hz, 2H, Pyr-H4 (equatorial), 8.7 (d, J = 4.96 Hz, 2H, Pyr-H6 (equatorial)), 8.97 (d, J = 5.09 Hz, 1H, Pyr H6 (axial)). Anal. Calcd for $C_{20}H_{23}F_6N_4O_9S_2Ru$: C, 32.35; H, 3.12; N, 7.54. Found: C, 32.66; H, 3.00; N, 7.62. Absorption maxima (λ_{max}, nm): 338, 404, 604.

[Ru(Me$_3$TPA)(H$_2$O)$_2$](CF$_3$SO$_3$)$_2$ (2). Yield: 40%. ^{1}H NMR (270 MHz, CD$_3$CN): δ 2.92 (S, 9H, methyl), 4.25 (s, 6H, −CH$_2$−), 7.25 (d, J = 7.02 Hz, 1H, Pyr-H3 (axial)), 7.27 (d, J = 7.02 Hz, 2H, Pyr-H3 (equatorial)), 7.74 (d, J = 7.02 Hz, 1H Pyr-H4 (axial)), 7.76 (d, J = 7.01 Hz, 2H, Pyr-H4 (equatorial)), 8.34 (t, J = 7.02 Hz, 3H, Pyr-H5). Anal. Calcd for $C_{23}H_{28}F_6N_4O_8S_2Ru$: C, 35.98; H, 3.68; N, 7.30. Found: C, 36.41; H, 3.52; N, 7.40. Absorption maxima (λ_{max}, nm): 610 (br).

[RuCl(DPA-Bpy)]Cl·3H$_2$O·CH$_3$OH (3a·3H$_2$O·CH$_3$OH). To a refluxed solution of RuCl$_3$·3H$_2$O (0.17 g, 0.65 mmol) in 80 mL of ethanol was added dropwise a solution of DPA-Bpy (0.24 g, 0.65 mmol) in 10 mL of ethanol over a period of 25 min under an argon atmosphere. The reaction mixture was refluxed for 12 h. Crude reaction mixture was filtered to remove inorganic material present in solution. The filtrate was evaporated under reduced pressure and purified by dissolving in a minimum amount of methanol and then washed with 20 mL of diethyl ether to get the purified product as a precipitate, which was dried under reduced pressure to afford dark red solid (0.30 g, 73%). Crystals suitable for X-ray crystallography were grown by slow diffusion of ether into a

concentrated solution of the complex in acetonitrile. ^{1}H NMR (CD$_3$CN, 500 MHz): δ 4.90 (t, 2H, axial bipyridyl methylene, H6), 5.17 (d, 4H, equatorial pyridyl methylene, H1), 6.93 (t, J = 13.12 Hz, 2H, py-H4,), 7.15 (d, J = 7.7 Hz, 1H, bpy-H7), 7.17 (dt, J = 11.88, 5.45 Hz, 2H, py-H5), 7.37 (d, J = 7.91 Hz, 2H, Py-H2), 7.54 (t, J = 7.91 Hz, 1H, bpy-H8), 7.59 (dt, J = 7.91 Hz, 2H, Py-H3), 7.78 (dt, J = 14.09 Hz, 1H, bpy-H12), 8.14 (dt, J = 8.21 Hz, 1H, bpy-H9), 8.17 (d, J = 7.8 Hz, 1H, bpy-H11), 8.40 (d, J = 8.15 Hz, 1H, bpy-H10), 9.46 (d, J = 5.67 Hz, 1H, bpy-H13). ESI-MS: m/z 504.13 (calcd m/z^+ for $[M − Cl^-]^+$ 503.97). Anal. Calcd for $C_{24}H_{30}Cl_2N_5O_4Ru$: C, 46.16; H, 4.84; N, 11.21. Found: C, 46.35; H, 4.75; N, 11.23. Absorption maxima (λ_{max}) (CH$_2$Cl$_2$) (λ_{max}, nm): 384 (sh), 430, 516.

[Ru(DPA-Bpy)Cl](PF$_6$)·3H$_2$O. To a cold aqueous solution of 3a was added dropwise a saturated solution of NH$_4$PF$_6$. The reaction mixture was filtered, washed with cold water, and dried to yield [Ru(DPA-Bpy)Cl](PF$_6$)·3H$_2$O as a dark red solid (0.30 g, 73%). ESI-MS: m/z^+ 504.24 (calcd m/z^+ for $[M − Cl]^+$ 503.97). Anal. Calcd for $C_{23}H_{26}ClF_6N_5O_3PRu$: C, 39.35; H, 3.73; N, 9.98. Found: C, 39.48; H, 3.38; N, 9.90.

[Ru(DPA-Bpy)(H$_2$O)](PF$_6$)$_2$ (3b). To a solution of [Ru(DPA-Bpy)Cl](PF$_6$)·3H$_2$O (0.085 g, 0.13 mmol) in 10 mL of H$_2$O was added dropwise a solution of AgPF$_6$ (0.050 g, 0.20 mmol) in 2 mL of H$_2$O under an argon atmosphere. The reaction mixture was refluxed overnight, and the precipitate was filtered through Celite. After removal of solvent, the residue was dissolved in a minimum amount of methanol, washed with diethyl ether, and dried under reduced pressure to yield a reddish solid (0.068 g, 68%). ^{1}H NMR (CD$_3$CN, 500 MHz): δ 4.93 (t, 4 H, axial bipyridyl methylene-H6), 5.07 (d, 2 H, equatorial pyridyl methylene-H1), 7.06 (t, J = 6.6 Hz, 2H, py-H4), 7.28 (dd, J = 8.0 Hz, 1H, bpy-H7), 7.30 (dd, J = 5.3 Hz, 2H, py-H5), 7.51 (d, J = 7.64 Hz, 2H, py-H2), 7.75 (dt, J = 7.81 Hz, 2H, py-H3), 7.79 (dt, J = 8.1 Hz, 1H, bpy-H8), 7.86 (dt, J = 6.5 Hz, 1H, bpy-H12), 8.23 (dt, J = 7.8 Hz, 1H, bpy-H11), 8.25 (d, J = 7.8 Hz, 1H, bpy-H9), 8.52 (d, J = 7.82 Hz, 1H, bpy-H10), 9.22 (d, J = 5.42 Hz, 1H, bpy-H13). ESI-MS: m/z^+ 613.7 (calcd m/z^+ for $[M − H_2O - PF_6]^+$ 613.0). Anal. Calcd for $C_{23}H_{23}F_{12}N_5OP_2Ru$: C, 35.58; H, 2.99; N, 9.02. Found: C, 35.83; H, 2.95; N, 8.90. Absorption maxima (CH$_2$Cl$_2$) (λ_{max}, nm): 372 (sh), 410, 496.

Characterization Methods. UV−vis absorption spectra were measured in 18.2 MΩ Milli-Q H$_2$O at room temperature using a HP-8452A diode array spectrometer. ^{1}H NMR spectroscopy was conducted on a Joel 270 MHz or a Varian DirectDrive 500 MHz spectrometer. Cyclic voltammetric measurements were performed in 0.1 M Britton−Robinson buffer using a glassy carbon electrode, a platinum wire counter electrode, and a Ag/AgCl reference electrode. When a redox wave was not clear in cyclic voltammetry, square wave voltammetry was used to determine its redox potential. All oxygen evolution measurements were performed using a calibrated O$_2$ electrode (YSI 5300A). Generally, Ce(IV) solution (0.33 M) was rapidly added to a stirred 4.0 mM complex solution in a 10 mL round-bottom flask, and O$_2$ evolution was recorded over time. Analysis of dioxygen in a reaction headspace was conducted using a HP G1800A GCD system gas chromatography with an electron ionization detector. GC-MS monitoring of the formation of CO$_2$ and O$_2$ by complexes 1b, 2, and 3b (0.2 mM) was conducted in the presence of Ce^{IV} (0.66 M) in 1 M HNO$_3$. Elemental analyses were conducted by Atlantic Microlab, Inc., Atlanta, GA.

X-ray Structure Determination. Crystals of 3a were obtained from slow diffusion of diethyl ether into an acetonitrile solution containing 3a at room temperature. A Leica MZ 75 microscope was used to identify a suitable crystal with very well-defined faces with dimensions (max, intermediate, and min) 0.1 mm × 0.1 mm × 0.01 mm. The crystal mounted on a nylon loop was then placed in a cold nitrogen stream maintained at 110 K. A BRUKER D8-GADDS X-ray (three-circle) diffractometer was employed for crystal screening, unit cell determination, and data collection. The goniometer was controlled using the FRAMBO software suite.[11] The detector was set at 6.0 cm from the

Table 1. Experimental and Computed Redox Potentials of 1, 2, and 3 in Britton−Robinson Buffer at pH 7, $E_{1/2}$, V vs NHE

	$Ru^{III/II}$	$(Ru^{III/II})^c$	$Ru^{IV/III}$	$(Ru^{IV/III})^c$	$Ru^{V/IV}$	$(Ru^{V/IV})^c$	$Ru^{VI/V}$	$(Ru^{VI/V})^c$
$1a^a$	0.42	−0.12	0.72	0.30	0.90	0.55	NA	0.85
1b	0.42		0.73		0.97		1.20	
2	0.26	0.00	0.62	0.24	1.00	0.63	1.36	0.83
3b	0.60	0.26	0.84	0.56	NA		NA	
$3b^b$	0.89		1.20		1.75		NA	

^{a} From ref 9. ^{b} In 0.1 M HNO_3. ^{c} Computed redox potential.

crystal sample (MWPC Hi-Star Detector, 512 × 512 pixel). X-ray radiation employed was generated from a Cu sealed X-ray tube (Cu $K\alpha$ = 1.54184 Å with a potential of 40 kV and a current of 40 mA) fitted with a graphite monochromator in the parallel mode (175 mm collimator with 0.5 mm monocapillary optics).

Data Reduction, Structure Solution, and Refinement. Integrated intensity information for each reflection was obtained by reduction of the data frames with the program SAINT.[12] The integration method employed a three-dimensional profiling algorithm, and all data were corrected for Lorentz and polarization factors as well as for crystal decay effects. Finally, the data was merged and scaled to produce a suitable data set. The absorption correction program SADABS was employed to correct the data for absorption effects.[13]

Systematic reflection conditions and statistical tests for the data suggested the space group $P1$. A solution was obtained readily using SHELXTL (SHELXS).[14] All non-hydrogen atoms were refined with anisotropic thermal parameters. The hydrogen atoms bound to carbon were placed in idealized positions [C−H = 0.96 Å, $U_{iso}(H)$ = 1.2 × $U_{iso}(C)$]. The structure was refined (weighted least-squares refinement on F^2) to convergence.[13] X-seed was employed for final data presentation and structure plots.[15]

Density Functional Theory (DFT) Calculations and Computed Redox Potentials. The redox potentials were calculated using a method similar to the one devised by Roy et al.[16] The computed free energy of solution, ΔG_{soln}^{comp}, is calculated from the free energy change in the gas phase of the redox couple, ΔG_{gas}^{redox}, the solvation free energy change between the oxidized (ΔG_{solv}^{comp} (ox)) and the reduced species (ΔG_{solv}^{comp} (red)), and the number of protons, lost from the complex to solution (n) (eq 1). In order to account for the loss of a proton to solvent water, the experimental value for the solvation of a proton (ΔG_{solv}^{exp} (H^+) = −265.9 kcal mol^{-1}, the value suggested by Truhlar[17]) and the gas-phase Gibbs free energy of a proton (ΔG_{gas}^{exp} (H^+) = −6.28 kcal mol^{-1})[18] were used.

$$\Delta G_{soln}^{comp} = \Delta G_{gas}^{redox, comp} + \Delta G_{solv}^{comp}(red) - \Delta G_{solv}^{comp}(ox) - n[\Delta G_{solv}^{exp}(H^+) + \Delta G_{gas}^{exp}(H^+)] \quad (1)$$

ΔG_{soln}^{comp} and the absolute value of the standard hydrogen electrode (SHE, also called the normal hydrogen electrode, NHE) in water (−4.44 ± 0.02 V)[19] are used to determine the standard one-electron redox potential, $E_{soln}^{\circ,comp}$, where F is the Faraday constant, 23.06 kcal mol^{-1} V^{-1} (eq 2).

$$E_{soln}^{\circ, comp} = \frac{\Delta G_{soln}^{comp}}{-23.06 \frac{kcal}{mol \cdot V}} - 4.44 \text{ V} \quad (2)$$

The computed oxidation potentials the ruthenium species in water are shown in Table 1 with results referenced to the absolute value of the standard hydrogen electrode (SHE) in water.

Theoretical calculations were carried out using Gaussian 03[20] and Gaussian 09.[21] Density functional theory[22] PBE [PBE exchange functional and correlation functional[23]] and M06[24] functionals with the default pruned fine grids for energies (75, 302), default pruned course grids for gradients and Hessians (35, 110) [neither grid is pruned for

ruthenium], and nondefault SCF convergence for geometry optimizations (10^{-6}). All PBE calculations were carried out using Gaussian 03. All M06 calculations were carried out using Gaussian 09.[25] The basis sets utilized were the LANL08,[26] which is a triple-ζ-modified version of the original Hay−Wadt basis set with an ECP for ruthenium, and 6-311G-(d)[27] basis set for all other atoms. The density fitting approximation[28] for the fitting of the Coulomb potential was used for all PBE calculations; auxiliary density-fitting basis functions were generated automatically (by the procedure implemented in Gaussian 03) for the specified AO basis set. The Hessian was computed on gas-phase-optimized geometries, and standard statistical mechanical relationships were used to determine the change in Gibbs free energy in the gas phase, ΔG_{gas}. The solvation free energies, ΔG_{solv}^{comp}, were calculated using two different methods, C-PCM[29] and SMD.[30] The C-PCM method was used to compute solvation free energies via the self-consistent reaction field (SCRF) keyword in Gaussian 03.[29b] The solvent cavity was built using the universal force field (UFF) radii from the UFF force field,[31] as recommended by Roy et al. for this computational scheme.[16] In Gaussian 03 solvent calculations, the SCFVAC keyword was used and solvent parameters consistent with water were used to model implicit solvation by the solvent. All other default solvent parameters for water were used. The SMD method was used to compute solvation free energies via the self-consistent reaction field (SCRF) keyword for M06 in Gaussian 09. The SMD solvation model was used with the default parameters consistent with water as the solvent. The results from the PBE functional with C-PCM solvation free energies gave a superior linear correlation with the experimental values; therefore, the results from the M06 functional with SMD solvation free energies are not discussed further and are given in the Supporting Information (Figure S1).

■ RESULTS AND DISCUSSION

Synthesis and Structure. Complex **1a** was synthesized following literature method from reaction of bis-μ-chloro Ru^{II} dimer, $[RuCl(TPA)]_2(PF_6)_2$, with $AgPF_6$ under refluxing conditions.[8,9] However, attempts to synthesize the tris(6-methyl-2-pyridylmethyl)amine (Me_3TPA) analog of the bis-μ-chloro Ru^{II} dimer resulted in a low yield. We prepared mononuclear Ru^{II} complexes $[Ru(TPA)(H_2O)_2](OTf)_2 \cdot H_2O$ (**1b**) and $[Ru(Me_3TPA)(H_2O)_2](OTf)_2$ (**2**) from refluxing an ethanol solution containing $RuCl_3 \cdot 3H_2O$, AgOTf, and the corresponding ligand (TPA and Me_3TPA).

Bipyridine (bpy) and its derivatives have been used widely in ruthenium catalysts for water oxidation.[5e,32] Since TPA is a tetradentate ligand, both complexes **1** and **2** have two coordinated H_2O molecules. In order to investigate the chelating effects of polydentate ligands on the stability of metal complexes toward water oxidation, we introduced a bpy group into TPA ligand to produce a new type of pentadentate ligand, N,N-bis(2-pyridinylmethyl)-2,2′-bipyridine-6-methanamine (DPA-Bpy). DPA-Bpy was synthesized from reaction of di-2-picolylamine and 6-(bromomethyl)-2,2′-bipyridine (Scheme 1).[10a] Reaction

of $RuCl_3 \cdot 3H_2O$ with DPA-Bpy in refluxing ethanol solution led to formation of a water-soluble complex [RuCl(DPA-Bpy)]Cl (**3a**). The coordinated Cl^- in **3a** could be substituted by a H_2O molecule to yield **3b** from refluxing an aqueous solution of **3a** in the presence of $AgPF_6$. Alternatively, complex **3b** can be prepared from reaction of 1 equiv of $AgPF_6$ with [RuCl(DPA-Bpy)](PF$_6$). The prepared compounds were characterized by elemental analysis, UV–vis, and 1D and 2D NMR (see the Supporting Information).

A single-crystal of complex **3a** was obtained from slow diffusion of diethyl ether into an acetonitrile solution containing **3a** at room temperature. The X-ray crystal structure of the cationic form of **3a** is shown in Figure 2, with the crystallographic parameters listed in Table S2, Supporting Information. As shown in Figure 2, the Ru center adopts a pseudooctahedral geometry with five positions occupied by the pentadentate ligand, DPA-Bpy, and the final position by Cl^-, which lies in a position cis to the tertiary amine group and the two pyridine moieties which are trans to each other. The selected bond distances and angles of **3a**

Scheme 1. Synthesis of DPA-Bpy Ligand and Complexes 3a and 3b
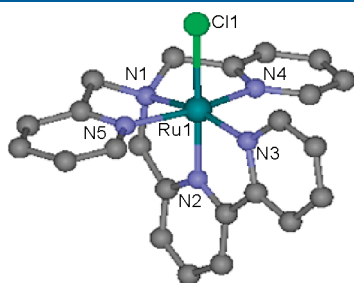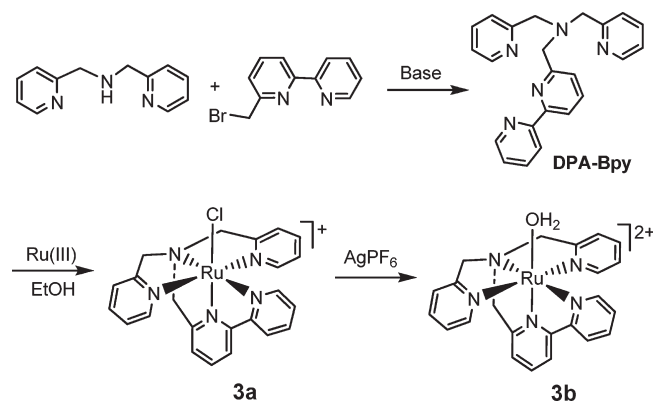
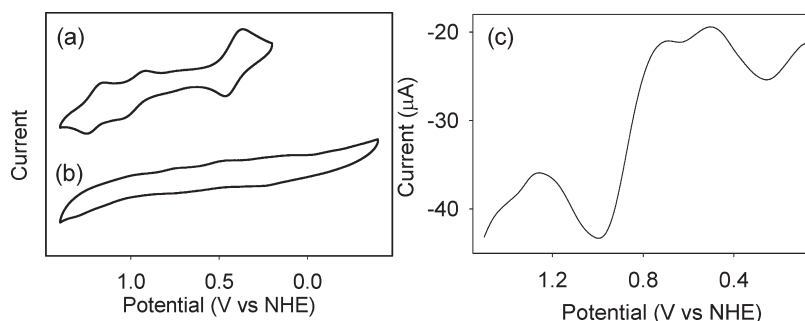**Figure 2.** X-ray structure of the cationic moiety of **3a**.
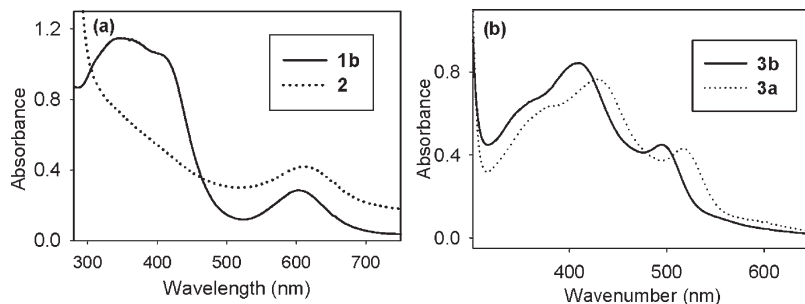
are shown in Table S3, Supporting Information. The two trans pyridine groups and the bipyridine group caused distortion of the Ru center from octahedral geometry, having $\angle$ N(5)–Ru(1)–N(4) = 164.1(5)° and $\angle$ N(1)–Ru(1)–N(3) = 164.5(5)°, respectively. The Ru–N and Ru–Cl distances are similar to those reported in the literature.[8,33]

1D and 2D NMR experiments were carried out to characterize all complexes in solution state, and the assignments of each resonance were accomplished based on their integration, multiplicity, and symmetry (see the Experimental Section and Supporting Information Figures S2–S5). As shown in Figure S3, Supporting Information, the ^1H NMR spectrum of complex **3a** shows the two pyridine groups have the same NMR features, indicating the presence of C_s symmetry for **3a** in solution with a plane containing the tertial amine and the bipyridine group. Such structural feature of **3a** in solution is consistent with its solid state X-ray structure. Table S1, Supporting Information, lists the comparison of each resonance in free ligand, DPA-Bpy, and its Ru complexes **3a** and **3b**. Compared to free DPA-Bpy, coordination of Ru caused the downfield shifts of all three methylene groups and H11–13 (Figure S3, Supporting Information). An upfield shift was clearly observed for H2, H5, H7, and H9 in both **3a** and **3b**.

Spectroscopic and Redox Properties. The UV–vis spectra of **1b** and **2** in water solution are displayed in Figure 3a, which showed slight changes in MLCT bands from the $Ru(d\pi) \rightarrow py(p\pi^*)$ transition, indicating the TPA and Me_3TPA ligands have similar π-acceptor character.[8] As seen from Figure 3b, substitution of Cl^- by a H_2O molecule shifts the absorption spectrum of **3a** in CH_2Cl_2 from 430 and 516 nm to 410 and 496 nm, respectively, in **3b**.

Previous studies have shown that compound **1a** at pH 7 exhibits a sequence of three redox events centered at 0.42, 0.72, and 0.90 V (vs NHE), corresponding to the $Ru^{III/II}$, $Ru^{IV/III}$, and $Ru^{V/IV}$ couples, respectively.[9] The electrochemical properties of complexes **1b**, **2**, and **3** were investigated in aqueous solution at pH 7 at room temperature. The cyclic voltammogram of **1b** at pH 7 exhibits a reversible $Ru^{III/II}$ couple at 0.42 V (vs NHE), the same as that reported for **1a** (Figure 4a). The barely visible $Ru^{IV/III}$ couple was determined to be 0.73 V from square wave voltammetry. The $Ru^{V/IV}$ and $Ru^{VI/V}$ couples appear at 0.97 and 1.20 V, respectively, similar to that previously observed for **1a**.[9] Compared to **1b**, the CV of **2** showed much weaker redox signals (Figure 4b). The potentials for the redox state changes of **2** from Ru^{II} to Ru^{VI} were determined by square wave voltammetry (Table 1 and Figure 4c). At pH 7, complex **3b** exhibits two reversible redox waves at 0.60 and 0.84 V, which were assigned to $Ru^{III/II}$ and $Ru^{IV/III}$, respectively. At pH 1 (0.1 M HNO_3), the corresponding redox potentials for the $Ru^{III/II}$ and $Ru^{IV/III}$

Figure 3. UV–vis spectra of (a) **1b** (solid line) and **2** (dotted line) in H_2O and (b) **3a** (dotted line) and **3b** (solid line) in CH_2Cl_2.

Figure 4. Cyclic voltammograms of (a) **1b** and (b) **2** and (c) square wave voltammogram of **2** in 100 mM Britton–Robinson buffer at pH 7: scan rate, 100 mV/s; working electrode, glassy carbon; counter electrode, Pt wire; reference electrode, Ag/AgCl.
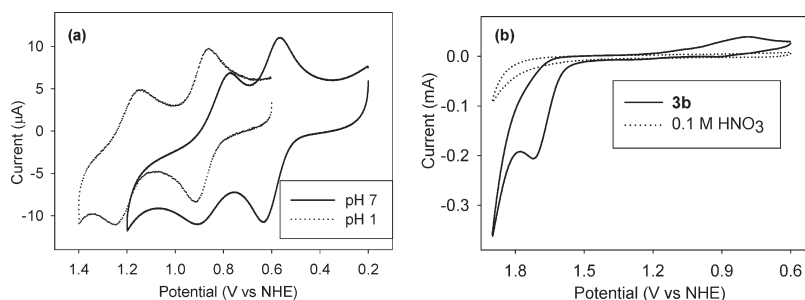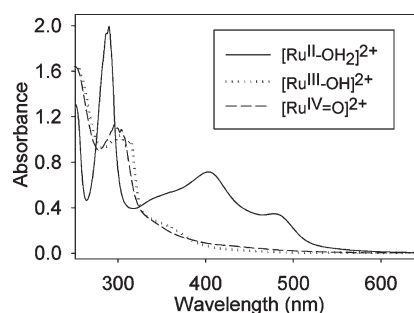

Figure 5. (a) Cyclic voltammograms of **3b** (1 mM) in 100 mM KPi buffer at pH 7 (solid line) and 0.1 M HNO$_3$ (dotted line). (b) Comparison of CV in the absence (dotted line) and presence (solid line) of **3b** (1 mM). Scan rate, 100 mV/s; working electrode, glassy carbon; counter electrode, Pt wire; reference electrode, Ag/AgCl.
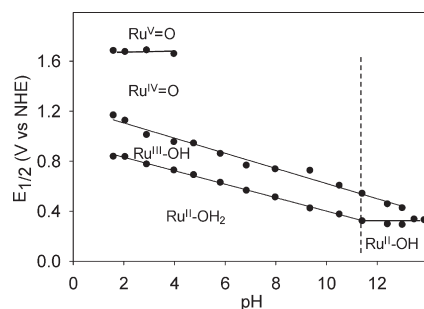
Figure 6. Pourbaix diagram for complex **3b** in aqueous Britton–Robinson buffer ($E_{1/2}$ vs Ag/AgCl).

Figure 7. UV–vis spectra of **3b** at different oxidation states: $[Ru^{II}-OH_2]^{2+}$ (solid line), $[Ru^{III}-OH]^{2+}$ (dotted line), and $[Ru^{IV}=O]^{2+}$ (dashed line) generated from stoichiometric oxidation with Ce^{IV} in 0.1 M HNO$_3$.

couples appear at 0.89 and 1.22 V, respectively (Figure 5a). Another shoulder assignable to the $Ru^{V/IV}$ couple appeared at 1.72 V before the catalytic wave of water oxidation at pH 1 (Figure 5b). The Pourbaix diagram for complex **3b** in the region of pH 1−14 is shown in Figure 6, with redox state changes from Ru^{II} to Ru^{V}. The $Ru^{III/II}$ couple is −54 mV/pH, and the $Ru^{IV/III}$ couple is −61 mV/pH, consistent with a proton-coupled electron transfer process which enables formation of a high-valent Ru=O species. The pK_a of coordinated H$_2$O in **3b** was determined to be 11.8 from pH titration in the range of pH 7−13 (Figure S6, Supporting Information), consistent with that observed the Pourbaix diagram of complex **3b**. The UV–vis spectral changes of **3b** at different oxidation states are reported in Figure 7. Addition of 1 equiv of Ce^{IV} to **3b** in 0.1 M HNO$_3$ resulted in a bleaching of the MLCT bands and the appearance of a broad peak at 350 nm. Further addition of 1 equiv of Ce^{IV} shifted the

350 nm peak to a weak band at 430 nm, corresponding to formation of $Ru^{IV}=O$ species.

Introduction of the CH$_3$ group on the pyridine ring is expected to reduce the redox potential of its metal centers because of the electron-donating ability of the CH$_3$ group. However, previous studies have shown that the metal complexes with α-substituted Me$_3$TPA ligand have higher redox potentials than those with TPA ligand.[7a,34] The unexpected observation is due to the steric effect of the 6-CH$_3$ substituent on pyridine, which could increase the bond length of the M−N$_{py}$ bond and result in a much weaker electron donor for 6-CH$_3$ pyridine.[7a,34] We carried out DFT calculations to investigate the effects of introducing a CH$_3$ group on the pyridine ring of TPA ligand on the redox potential of Ru complexes. The computed structures of $Ru^{IV}=O$ species for
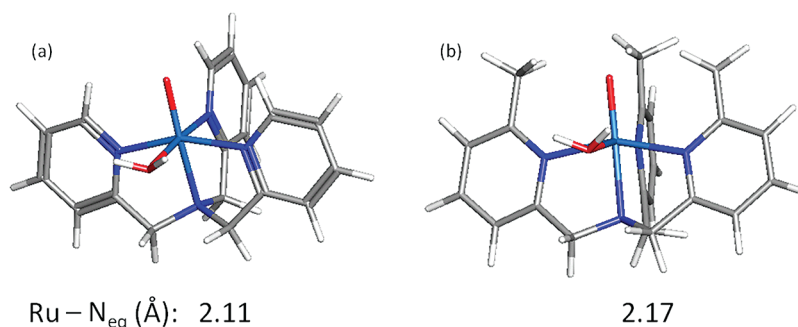
Figure 8. DFT-optimized structures for dicationic $Ru^{IV}=O$ species of (a) **1** and (b) **2**.
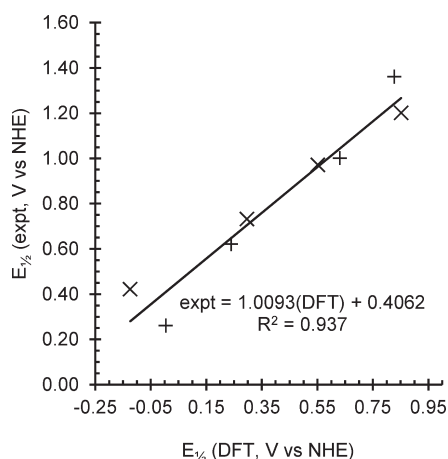

Figure 9. Linear relationship between the computed and the experimental redox potential for complexes **1** ($\times$) and **2** ($+$).

1 and **2** showed similar effects, with **2** having longer $Ru-N_{eq}$ bond distances (2.17 Å) than that of **1** (2.11 Å) (Figure 8). As shown in Table 1, DFT calculations predict that the $Ru^{V/IV}$ couple for **2** has a potential of $\sim$80 mV higher than that of **1**. The observed redox potentials for the $Ru^{V/IV}$ couple of **1** and **2** remain nearly unchanged, suggesting that the α-substituted Me_3TPA ligand has little effect on the redox potential of the Ru centers (Table 1). The trend in the computed redox potentials closely matches the trend observed in the experimental values redox potentials (Figure 9), suggesting DFT calculations can be used to predict the redox behavior of metal complexes and thus providing important guidelines for future studies.

Water Oxidation Studies. The oxygen evolution activity of complexes **1**–**3** was examined following literature methods using Ce^{IV} as oxidant ($2H_2O + 4Ce^{IV} \rightarrow O_2 + 4H^+ + 4Ce^{III}$), and the evolved oxygen was monitored using a calibrated O_2 electrode.[35] Addition of excess Ce^{IV} solution to 4.0 mM **1a** (3 mL) solution resulted in rapid production of O_2 (Figure S7a, Supporting Information). The evolved gas was confirmed to be O_2 by GC-MS, and the amount of O_2 produced was calculated to be $\sim$12 μmol, corresponding to formation of 1 equiv of O_2. When 97% $H_2^{18}O$ was used as a solvent, the appearance of a main peak at $m/z = 36$ was observed, suggesting formation of $^{18}O_2$ with $H_2^{18}O$ as the source of O_2 (Figure S7b, Supporting Information). Similar to that of **1a**, water oxidation by complex **1b** was investigated following the same procedure and the amount of O_2 produced was determined to be 1 O_2/Ru, suggesting that the triflate counterion has little effect on the water oxidation activity (Figure S8a,

Supporting Information). For complex **2**, we observed less than 10% of O_2 formation compared to that of **1**. This result could possibly be due to the steric effect of the CH_3 group. To test the water oxidation activity of **1** under neutral conditions, cyclic voltammetry of **1b** was performed in 100 mM sodium phosphate buffer at pH 7. As shown in Figure S8b, Supporting Information, the presence of **1b** in buffer resulted in a strong irreversible anodic current at potential higher than 1.5 V (vs NHE) due to the electrocatalytic oxidation of water to O_2. The observation of water oxidation at a potential higher than 1.5 V indicated that a high-valent $Ru(V)=O$ or higher oxidation state may be responsible for water oxidation. As shown in Figure 10a, the water oxidation activity of **3b** was determined with a turnover number of 24. Under the same conditions, complexes **1a** and **2** have much less activity in water oxidation. Therefore, there is a significant improvement in the water oxidation activity by introducing a bpy group in complex **1**. The activity of these complexes is relatively low in terms of turnover number and turnover frequency, in an order similar to that reported for mononuclear $[Ru(bpy)_2(H_2O)_2]^{2+}$.[36]

Decomposition of Ru catalysts under acidic conditions in Ce^{IV} solution has been noted, and a variety of pathways have been proposed to account for catalyst deactivation. Recently, Llobet and co-workers reported water oxidation by a series of tetranuclear Ru complexes and demonstrated that decomposition of methylene groups of tetranucleating ligands to CO_2 could be one possible pathway for deactivation of Ru catalysts.[37] Indeed, we also observed formation of CO_2 during the water oxidation process of **1**–**3**; this result is probably due to the presence of methylene groups in TPA ligand. In order to determine whether complexes **1**–**3** act as real catalysts or just precursors for water oxidation, we monitored the simultaneous formation of O_2 and CO_2 using GC-MS. As shown in Figure 10b, the rate of O_2 formation for complex **3b** is 12 times of that of CO_2 formation in the presence of excess Ce^{IV} in 1 M HNO_3. Under the same conditions, complex **1a** displays a rate of O_2 formation at 1.5 times that of CO_2 formation (Figure S9a, Supporting Information). However, the rate for CO_2 formation of complex **2** is 1.7 times that of O_2 formation (Figure S9b, Supporting Information); this result may explain the much lower water oxidation activity of **2** when compared to **1** and **3**. These results clearly demonstrated oxidation of water by complexes **1**–**3**, and simultaneous oxidation of ligand to CO_2 contributes to catalyst decomposition.

Oxidation of water by mononuclear Ru complexes has been demonstrated by a family of Ru complexes.[5g,35,36,38] The involvement of a high-valent $Ru=O$ species, presumably $Ru^V=O$, has been proposed as an active intermediate for oxidation of water. Oxidation of Ru^{II} to Ru^{IV} by the PCET process and its
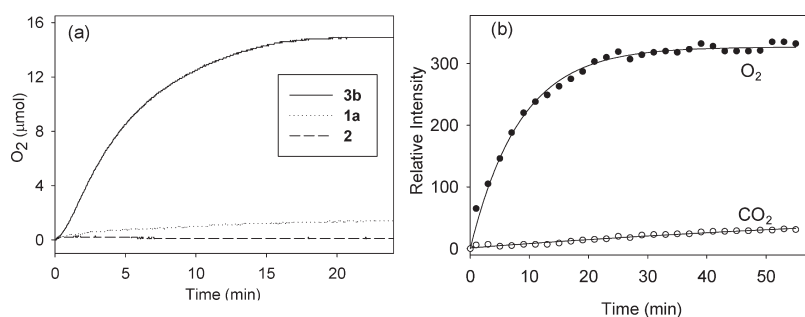
Figure 10. (a) Oxygen evolution vs time after addition of 0.33 M Ce^{IV} to 3 mL of 0.2 mM complexes **1a** (dotted line), **2** (dashed line), and **3b** (solid line) in 1 M HNO_3. (b) GC-MS monitoring of the formation of O_2 and CO_2 during the catalytic oxidation of water by **3b** (0.2 mM) in the presence of Ce^{IV} (0.33 M) in 1 M HNO_3.

Scheme 2. Proposed Mechanism for Water Oxidation by Mononuclear Ru Complex
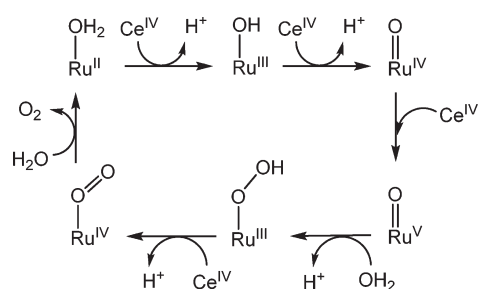
further oxidation to $Ru^V=O$ may trigger oxidation of water to produce a peroxo-bound intermediate $(Ru^{III}-O-O-H)$, which can be oxidized with release of a proton and molecular O_2 (Scheme 2).

SUMMARY

We have prepared and characterized new types of mononuclear Ru complexes with tripodal TPA tetradentate-ligand and DPA-Bpy pentadentate-ligand architectures. Compared to Ru complexes with the tetradentate TPA ligand, Ru complexes with the new pentadentate DPA-Bpy ligand have significantly increased stability and catalytic activity for water oxidation. While TPA ligand and its derivatives have been widely used in designing metal complexes for O_2 activation, our studies have demonstrated that Ru complexes with TPA, TPA derivatives, and DPA-Bpy produce O_2 from water oxidation, demonstrating the versatile reactivities of TPA and DPA-Bpy ligand architectures when bound with different metal ions.[39] Further mechanistic studies of water oxidation by $[Ru(TPA)(H_2O)_2]^{2+}$, $[Ru(Me_3TPA)(H_2O)_2]^{2+}$, and $[Ru(DPA-Bpy)(H_2O)]^{2+}$ complexes (**1**, **2**, and **3**, respectively) and further modifications of TPA and DPA-Bpy ligands to improve the water oxidation activity of their metal complexes are currently in progress.

ASSOCIATED CONTENT

Ⓢ Supporting Information. 1D and 2D NMR spectra, further results for calculation of redox potentials with DFT, oxygen evolution figures, and crystallographic data in CIF format; complete list for refs 20 and 21. This material is available free of charge via the Internet at http://pubs.acs.org.

AUTHOR INFORMATION

Corresponding Author
*Email: cewebstr@memphis.edu; xzhao1@memphis.edu.

ACKNOWLEDGMENT

REFERENCES

(1) Eisenberg, R.; Gray, H. B. *Inorg. Chem.* **2008**, *47*, 1697–1699.

(2) (a) Barber, J. *Biochem. Soc. Trans.* **2006**, *34*, 619–631. (b) Renger, G. *Biochim. Biophys. Acta* **2001**, *1503*, 210–228.

(3) (a) Lewis, N. S.; Nocera, D. G. *Proc. Natl. Acad. Sci. U.S.A.* **2006**, *103*, 15729–15735. (b) Hoertz, P. G.; Mallouk, T. E. *Inorg. Chem.* **2005**, *44*, 6828–6840.

(4) (a) Mukhopadhyay, S.; Mandal, S. K.; Bhaduri, S.; Armstrong, W. H. *Chem. Rev.* **2004**, *104*, 3981–4026. (b) Dau, H.; Limberg, C.; Reier, T.; Risch, M.; Roggan, S.; Strasser, P. *ChemCatChem* **2010**, *2*, 724–761.

(5) (a) Yagi, M.; Narita, K. *J. Am. Chem. Soc.* **2004**, *126*, 8084–8085. (b) Poulsen, A. K.; Rompel, A.; McKenzie, C. J. *Angew. Chem., Int. Ed.* **2005**, *44*, 6916–6920. (c) Limburg, J.; Vrettos, J. S.; Liable-Sands, L. M.; Rheingold, A. L.; Crabtree, R. H.; Brudvig, G. W. *Science* **1999**, *283*, 1524–1527. (d) Brimblecombe, R.; Swiegers, G. F.; Dismukes,

G. C.; Spiccia, L. *Angew. Chem., Int. Ed.* **2008**, *47*, 7335–7338. (e) Gersten, S. W.; Samuels, G. J.; Meyer, T. J. *J. Am. Chem. Soc.* **1982**, *104*, 4029–4030. (f) Gilbert, J. A.; Eggleston, D. S.; Murphy, W. R., Jr.; Geselowitz, D. A.; Gersten, S. W.; Hodgson, D. J.; Meyer, T. J. *J. Am. Chem. Soc.* **1985**, *107*, 3855–3864. (g) Zong, R.; Thummel, R. P. *J. Am. Chem. Soc.* **2005**, *127*, 12802–12803. (h) Geletii, Y. V.; Botar, B.; Kogerler, P.; Hillesheim, D. A.; Musaev, D. G.; Hill, C. L. *Angew. Chem., Int. Ed.* **2008**, *47*, 3896–3899. (i) Kanan, M. W.; Nocera, D. G. *Science* **2008**, *321*, 1072–1075. (j) McEvoy, J. P.; Brudvig, G. W. *Phys. Chem. Chem. Phys.* **2004**, *6*, 4754–4763. (k) Pecoraro, V. L.; Baldwin, M. J.; Caudle, M. T.; Hsieh, W.-Y.; Law, N. A. *Pure Appl. Chem.* **1998**, *70*, 925–929. (l) Limburg, J.; Szalai, V. A.; Brudvig, G. W. *J. Chem. Soc., Dalton Trans.* **1999**, 1353–1362. (m) Betley, T. A.; Wu, Q.; Van Voorhis, T.; Nocera, D. G. *Inorg. Chem.* **2008**, *47*, 1849–1861. (n) McEvoy, J. P.; Brudvig, G. W. *Chem. Rev.* **2006**, *106*, 4455–4483. (o) Hull, J. F.; Balcells, D.; Blakemore, J. D.; Incarvito, C. D.; Eisenstein, O.; Brudvig, G. W.; Crabtree, R. H. *J. Am. Chem. Soc.* **2009**, *131*, 8730–8731.

(6) (a) Muckerman, J. T.; Polyansky, D. E.; Wada, T.; Tanaka, K.; Fujita, E. *Inorg. Chem.* **2008**, *47*, 1787–1802. (b) Hurst, J. K.; Cape, J. L.; Clark, A. E.; Das, S.; Qin, C. *Inorg. Chem.* **2008**, *47*, 1753–1764. (c) Deng, Z. P.; Tseng, H. W.; Zong, R. F.; Wang, D.; Thummel, R. *Inorg. Chem.* **2008**, *47*, 1835–1848. (d) Liu, F.; Concepcion, J. J.; Jurss, J. W.; Cardolaccia, T.; Templeton, J. L.; Meyer, T. J. *Inorg. Chem.* **2008**, *47*, 1727–1752. (e) Mola, J.; Mas-Marza, E.; Sala, X.; Romero, I.; Rodriguez, M.; Vinas, C.; Parella, T.; Llobet, A. *Angew. Chem., Int. Ed.* **2008**, *47*, 5830–5832. (f) Concepcion, J. J.; Jurss, J. W.; Norris, M. R.; Chen, Z.; Templeton, J. L.; Meyer, T. J. *Inorg. Chem.* **2010**, *49*, 1277–1279. (g) Duan, L. L.; Fischer, A.; Xu, Y. H.; Sun, L. C. *J. Am. Chem. Soc.* **2009**, *131*, 10397–10399. (h) Yoshida, M.; Masaoka, S.; Sakai, K. *Chem. Lett.* **2009**, *38*, 702–703.

(7) (a) Zang, Y.; Kim, J.; Dong, Y.; Wilkinson, E. C.; Appelman, E. H.; Que, L., Jr. *J. Am. Chem. Soc.* **1997**, *119*, 4197–4205. (b) Nagao, H.; Komeda, N.; Mukaida, M.; Suzuki, M.; Tanaka, K. *Inorg. Chem.* **1996**, *35*, 6809–6815. (c) Suzuki, M. *Acc. Chem. Res.* **2007**, *40*, 609–617. (d) Que, L., Jr.; Dong, Y. *Acc. Chem. Res.* **1996**, *29*, 190–196. (e) Jacobson, R. R.; Tyeklar, Z.; Farooq, A.; Karlin, K. D.; Liu, S.; Zubieta, J. *J. Am. Chem. Soc.* **1988**, *110*, 3690–3692.

(8) Kojima, T.; Amano, T.; Ishii, Y.; Ohba, M.; Okaue, Y.; Matsuda, Y. *Inorg. Chem.* **1998**, *37*, 4076–4085.

(9) Hirai, Y.; Kojima, T.; Mizutani, Y.; Shiota, Y.; Yoshizawa, K.; Fukuzumi, S. *Angew. Chem., Int. Ed.* **2008**, *47*, 5772–5776.

(10) (a) Tyeklar, Z.; Jacobson, R. R.; Wei, N.; Murthy, N. N.; Zubieta, J.; Karlin, K. D. *J. Am. Chem. Soc.* **1993**, *115*, 2677–2689. (b) Gultneh, Y.; Yisgedu, T. B.; Tesema, Y. T.; Butcher, R. J. *Inorg. Chem.* **2003**, *42*, 1857–1867. (c) Murashima, T.; Tsukiyama, S.; Fujii, S.; Hayata, K.; Sakai, H.; Miyazawa, T.; Yamada, T. *Org. Biomol. Chem.* **2005**, *3*, 4060–4064.

(11) *APEX2, Program for Data Collection on Area Detectors*; BRUKER AXS Inc.: Madison, WI, 2007.

(12) *SAINT, Program for Data Reduction from Area Detectors*; BRUKER AXS Inc.: Madison, WI, 2007.

(13) Sheldrick, G. M. *SADABS, Program for Absorption Correction of Area Detector Frames*; BRUKER AXS Inc.: Madison, WI, 2003.

(14) Sheldrick, G. M. *Acta Crystallogr., Sect. A* **2008**, *64*, 112–122.

(15) Barbour, L. J. *J. Supramol. Chem.* **2003**, *1*, 189–191.

(16) Roy, L. E.; Jakubikova, E.; Guthrie, M. G.; Batista, E. R. *J. Phys. Chem. A* **2009**, *113*, 6745–6750.

(17) Kelly, C. P.; Cramer, C. J.; Truhlar, D. G. *J. Phys. Chem. B* **2006**, *110*, 16066–16081.

(18) Moser, A.; Range, K.; York, D. M. *J. Phys. Chem. B* **2010**, *114*, 13911–13921.

(19) Trasatti, S. *Pure Appl. Chem.* **1986**, *58*, 955–966.

(20) Frisch, M. J., et al. *Gaussian 03*, revision C.02; Gaussian, Inc.: Wallingford, CT, 2004.

(21) Frisch, M. J., et al. *Gaussian 09*, revision A.02; Gaussian, Inc.: Wallingford, CT, 2009.

(22) Parr, R. G.; Yang, W. P. *Density Functional Theory of Atoms and Molecules*; Oxford University Press: New York, 1989.

(23) (a) Perdew, J. P.; Burke, K.; Ernzerhof, M. *Phys. Rev. Lett.* **1996**, *77*, 3865–3868. (b) Perdew, J. P.; Burke, K.; Ernzerhof, M. *Phys. Rev. Lett.* **1997**, *78*, 1396.

(24) Zhao, Y.; Truhlar, D. G. *Theor. Chem. Acc.* **2008**, *120*, 215–241.

(25) A reviewer asked for a comparison to the computed results from the M06 functional.

(26) Roy, L. E.; Hay, P. J.; Martin, R. L. *J. Chem. Theory Comput.* **2008**, *4*, 1029–1031.

(27) Krishnan, R.; Binkley, J. S.; Seeger, R.; Pople, J. A. *J. Chem. Phys.* **1980**, *72*, 650–654.

(28) (a) Dunlap, B. I. *J. Chem. Phys.* **1983**, *78*, 3140–3142. (b) Dunlap, B. I. *J. Mol. Struct.: Theochem* **2000**, *529*, 37–40. (c) Dunlap, B. I.; Connolly, J. W. D.; Sabin, J. R. *J. Chem. Phys.* **1979**, *71*, 3396–3402. (d) Dunlap, B. I.; Connolly, J. W. D.; Sabin, J. R. *J. Chem. Phys.* **1979**, *71*, 4993–4999.

(29) (a) Barone, V.; Cossi, M. *J. Phys. Chem. A* **1998**, *102*, 1995–2001. (b) Cossi, M.; Rega, N.; Scalmani, G.; Barone, V. *J. Comput. Chem.* **2003**, *24*, 669–681.

(30) Marenich, A. V.; Cramer, C. J.; Truhlar, D. G. *J. Phys. Chem. B* **2009**, *113*, 6378–6396.

(31) Rappe, A. K.; Casewit, C. J.; Colwell, K. S.; Goddard, W. A., III; Skiff, W. M. *J. Am. Chem. Soc.* **1992**, *114*, 10024–10035.

(32) Brudvig, G. W. *Philos. Trans. R. Soc. London, Ser. B: Biol. Sci.* **2008**, *363*, 1211–1219.

(33) Rodríguez, M.; Romero, I.; Llobet, A.; Deronzier, A.; Biner, M.; Parella, T.; Stoeckli-Evans, H. *Inorg. Chem.* **2001**, *40*, 4150–4156.

(34) (a) Benhamou, L.; Lachkar, M.; Mandon, D.; Welter, R. *Dalton Trans.* **2008**, 6996–7003. (b) Goodson, P. A.; Oki, A. R.; Glerup, J.; Hodgson, D. J. *J. Am. Chem. Soc.* **1990**, *112*, 6248–6254. (c) Hayashi, Y.; Kayatani, T.; Sugimoto, H.; Suzuki, M.; Inomata, K.; Uehara, A.; Mizutani, Y.; Kitagawa, T.; Maeda, Y. *J. Am. Chem. Soc.* **1995**, *117*, 11220–11229.

(35) Concepcion, J. J.; Jurss, J. W.; Templeton, J. L.; Meyer, T. J. *J. Am. Chem. Soc.* **2008**, *130*, 16462–16463.

(36) Sala, X.; Ertem, M. Z.; Vigara, L.; Todorova, T. K.; Chen, W.; Rocha, R. C.; Aquilante, F.; Cramer, C. J.; Gagliardi, L.; Llobet, A. *Angew. Chem., Int. Ed.* **2010**, *49*, 7745–7747.

(37) Francás, L.; Sala, X.; Escudero-Adán, E.; Benet-Buchholz, J.; Escriche, L. s.; Llobet, A. *Inorg. Chem.* **2011**, *50*, 2771–2781.

(38) Wasylenko, D. J.; Ganesamoorthy, C.; Henderson, M. A.; Koivisto, B. D.; Osthoff, H. D.; Berlinguette, C. P. *J. Am. Chem. Soc.* **2010**, *132*, 16094–16106.

(39) After submission of this article, a report by Fillol, Costas, and coworkers was published on an analogous FeTPA complex that has high activity for water oxidation, see: Fillol, J. L.; Codolà, Z.; Garcia-Bosch, I.; Gómez, L.; Pla, J. J.; Costas, M. *Nature Chem.* **2011**, *3*, 807–813.